Global optimization of omnidirectional wavelength selective emitters/absorbers based on dielectric-filled anti-reflection coated two-dimensional metallic photonic crystals

Yi Xiang Yeng,[1,2,*] **Jeffrey B. Chou,**[3] **Veronika Rinnerbauer,**[1] **Yichen Shen,**[1,4] **Sang-Gook Kim,**[3] **John D. Joannopoulos,**[1,2,4] **Marin Soljačić,**[1,2,4] **and Ivan Čelanović**[2]

[1]*Research Laboratory of Electronics, Massachusetts Institute of Technology, Cambridge, Massachusetts 02139, USA*
[2]*Institute of Soldier Nanotechnologies, Massachusetts Institute of Technology, Cambridge, Massachusetts 02139, USA*
[3]*Department of Mechanical Engineering, Massachusetts Institute of Technology, Cambridge, Massachusetts 02139, USA*
[4]*Department of Physics, Massachusetts Institute of Technology, Cambridge, Massachusetts 02139, USA*
[*]*yxyeng@mit.edu*

Abstract: We report the design of dielectric-filled anti-reflection coated (ARC) two-dimensional (2D) metallic photonic crystals (MPhCs) capable of omnidirectional, polarization insensitive, wavelength selective emission/absorption. Using non-linear global optimization methods, optimized hafnium oxide (HfO_2)-filled ARC 2D Tantalum (Ta) PhC designs exhibiting up to 26% improvement in emittance/absorptance at wavelengths λ below a cutoff wavelength λ_c over the unfilled 2D TaPhCs are demonstrated. The optimized designs possess high hemispherically average emittance/absorptance ε_H of 0.86 at $\lambda < \lambda_c$ and low ε_H of 0.12 at $\lambda > \lambda_c$.

OCIS codes: (350.4238) Nanophotonics and photonic crystals; (290.6815) Thermal emission; (300.1030) Absorption; (300.2140) Emission; Selective emitters/absorbers.

References and links

1. Y. X. Yeng, W. R. Chan, V. Rinnerbauer, J. D. Joannopoulos, M. Soljačić, and I. Čelanović, "Performance analysis of experimentally viable photonic crystal enhanced thermophotovoltaic systems," Opt. Express **21**, A1035–A1051 (2013).
2. C. E. Kennedy and H. Price, "Progress in Development of High-Temperature Solar-Selective Coating," in *International Solar Energy Conference* (ASME, 2005), pp. 749–755.
3. A. Tittl, P. Mai, R. Taubert, D. Dregely, N. Liu, and H. Giessen, "Palladium-based plasmonic perfect absorber in the visible wavelength range and its application to hydrogen sensing," Nano Lett. **11**, 4366–4369 (2011).
4. M. J. Blanco, J. G. Martín, and D. C. Alarcón-Padilla, "Theoretical efficiencies of angular-selective non-concentrating solar thermal systems," Solar Energy **76**, 683–691 (2004).
5. J.-J. Greffet, R. Carminati, K. Joulain, J.-P. Mulet, S. Mainguy, and Y. Chen, "Coherent emission of light by thermal sources," Nature **416**, 61–64 (2002).
6. I. Čelanović, D. Perreault, and J. Kassakian, "Resonant-cavity enhanced thermal emission," Phys. Rev. B **72**, 075127 (2005).

#212642 - $15.00 USD Received 23 May 2014; revised 12 Aug 2014; accepted 12 Aug 2014; published 29 Aug 2014

7. A. Heinzel, V. Boerner, A. Gombert, B. Bläsi, V .Wittwer, and J. Luther, "Radiation filters and emitters for the NIR based on periodically structured metal surfaces," J. Mod. Opt. **47**, 2399–2419 (2000).
8. M. U. Pralle, N. Moelders, M. P. McNeal, I. Puscasu, A. C. Greenwald, J. T. Daly, E. A. Johnson, T. George, D. S. Choi, I. El-Kady, and R. Biswas, "Photonic crystal enhanced narrow-band infrared emitters," Appl. Phys. Lett. **81**, 4685-4687 (2002).
9. H. Sai, Y. Kanamori, and H. Yugami, "High-temperature resistive surface grating for spectral control of thermal radiation," Appl. Phys. Lett. **82**, 1685–1687 (2003).
10. N. Liu, M. Mesch, T. Weiss, M. Hentschel, and H. Giessen, "Infrared perfect absorber and its application as plasmonic sensor," Nano Lett. **10**, 2342–2348 (2010).
11. Y. X. Yeng, M. Ghebrebrhan, P. Bermel, W. R. Chan, J. Joannopoulos, M. Soljačić, and I. Čelanović, "Enabling high temperature nanophotonics for energy applications," Proc. Natl. Acad. Sci. USA **109**, 2280–2285 (2011).
12. S. Y. Lin, J. Moreno, and J. G. Fleming, "Three-dimensional photonic-crystal emitter for thermal photovoltaic power generation," Appl. Phys. Lett. **83**, 380–382 (2003).
13. T. A. Walsh, J. A. Burr, Y.-S. Kim, T.-M. Lu, and S.-Y. Lin, "High-temperature metal coating for modification of photonic band edge position," J. Opt. Soc. Am. B **26**, 1450–1455 (2009).
14. S. E. Han and D. J. Norris, "Beaming thermal emission from hot metallic bull's eyes," Opt. Express **18**, 4829–4837 (2010).
15. T. V. Teperik, F. J. García de Abajo, A. G. Borisov, M. Abdelsalam, P. N. Bartlett, Y. Sugawara, and J. J. Baumberg, "Omnidirectional absorption in nanostructured metal surfaces," Nature Photonics **2**, 299–301 (2008).
16. B. Zhao and Z. M. Zhang, "Study of magnetic polaritons in deep gratings for thermal emission control," J. Quant. Spectrosc. Radiat. Transfer **135**, 81–89 (2014).
17. N. P. Sergeant, O. Pincon, M. Agrawal, and P. Peumans, "Design of wide-angle solar-selective absorbers using aperiodic metal-dielectric stacks," Opt. Express **17**, 22800–22812 (2009).
18. E. Rephaeli and S. Fan, "Absorber and emitter for solar thermo-photovoltaic systems to achieve efficiency exceeding the Shockley-Queisser limit," Opt. Express **17**, 15145–15159 (2009).
19. M. Ghebrebrhan, P. Bermel, Y. X. Yeng, J. D. Joannopoulos, M. Soljačić, and I. Čelanović, "Tailoring thermal emission via Q-matching of photonic crystal resonances," Phys. Rev. A **83**, 033810 (2011).
20. V. Rinnerbauer, Y. X. Yeng, W. R. Chan, J. J. Senkevich, J. D. Joannopoulos, M. Soljačić, and I. Čelanović, "High-temperature stability and selective thermal emission of polycrystalline tantalum photonic crystals," Opt. Express **21**, 11482–11491 (2013).
21. V. Rinnerbauer, S. Ndao, Y. X. Yeng, J. J. Senkevich, K. F. Jensen, J. D. Joannopoulos, M. Soljačić, I. Čelanović, and R. D. Geil, "Large-area fabrication of high aspect ratio tantalum photonic crystals for high-temperature selective emitters," J. Vac. Sci. Technol. B **31**, 011802 (2013).
22. V. Liu and S. Fan, "A free electromagnetic solver for layered periodic structures," Comput. Phys. Comm. **183**, 2233–2244 (2012).
23. A. F. Oskooi, D. Roundy, M. Ibanescu, P. Bermel, J. D. Joannopoulos, and S. G. Johnson, "Meep: A flexible free-software package for electromagnetic simulations by the FDTD method," Comp. Phys. Commun. **181**, 687-702 (2010).
24. P. Bermel, M. Ghebrebrhan, W. Chan, Y. X. Yeng, M. Araghchini, R. Hamam, C. H. Marton, K. F. Jensen, M. Soljačić, J. D. Joannopoulos, S. G. Johnson, and I. Čelanović, "Design and global optimization of high-efficiency thermophotovoltaic systems," Opt. Express **18**, A314–A334 (2010).
25. S. Kucherenko and Y. Sytsko, "Application of deterministic low-discrepancy sequences in global optimization," Comput. Optim. Appl. **30**, 297–318 (2005).
26. M. J. D. Powell, *Advances in Optimization and Numerical Analysis* (Kluwer Academic, 1994).
27. W. L. Price, "Global optimization by controlled random search," J. Optim. Theory Appl. **40**, 333–348 (1983).
28. S. G. Johnson, "The NLopt nonlinear-optimization package," http://ab-initio.mit.edu/nlopt.
29. J. B. Chou, Y. X. Yeng, A. Lenert, V. Rinnerbauer, I. Čelanović, M. Soljačić, E. N. Wang, and S.-G. Kim, "Design of wide-angle selective absorbers/emitters with dielectric filled metallic photonic crystals for energy applications," Opt. Express **22**, A144–A154 (2013).
30. H.-J. Lee, K. Smyth, S. Bathurst, J. Chou, M. Ghebrebrhan, J. Joannopoulos, N. Saka, and S.-G. Kim, "Hafnia-plugged microcavities for thermal stability of selective emitters," Appl. Phys. Lett. **102**, 241904 (2013).
31. F. L. Martínez, M. Toledano-Luque, J. J. Gandía, J. Cárabe, W. Bohne, J. Röhrich, E. Strub, and I. Mártil, "Optical properties and structure of HfO_2 thin films grown by high pressure reactive sputtering," J. Phys. D: Appl. Phys. **40**, 5256–5265 (2007).
32. H. R. Philipp, "The infrared optical properties of SiO_2 and SiO_2 layers on silicon," J. Appl. Phys. **50**, 1053–1057 (1979).
33. F. O'Sullivan, I. Čelanović, N. Jovanović, J. Kassakian, S. Akiyama, and K. Wada, "Optical characteristics of one-dimensional Si/SiO_2 photonic crystals for thermophotovoltaic applications," J. Appl. Phys. **97**, 033529 (2005).
34. T. D. Rahmlow, J. E. Lazo-Wasem, E. J. Gratrix, P. M. Fourspring, and D. M. Depoy, "New performance levels for TPV front surface filters," in *6th Thermophotovoltaic Generation of Electricity Conference* (AIP, 2004), pp. 180–188.

#212642 - $15.00 USD Received 23 May 2014; revised 12 Aug 2014; accepted 12 Aug 2014; published 29 Aug 2014

1. Introduction

Thermal radiation of naturally occurring materials is usually broadband and has a magnitude far weaker compared to the blackbody, rendering it inefficient for many applications including thermophotovoltaic (TPV) energy conversion [1], solar absorption [2], and chemical sensing [3]. For many of these applications, it is desirable to accurately control thermal emission (absorption) such that it occurs only in certain wavelength ranges over an optimum angular profile. For instance, TPV benefits from the use of omnidirectional selective emitters [1], while angularly selective absorption results in a more efficient solar absorber [4].

With the recent advancements in nanofabrication, various one-dimensional (1D) [3, 5, 6], 2D [7–11], and 3D [12,13] periodic structures have been investigated in order to obtain selective thermal emission. The first class of these relies on excitation of surface phonon-polaritons [5], surface plasmon-polaritons [3, 8, 10, 14], and localized plasmon resonances [15]. These mechanisms usually result in very sharp and narrow thermal emission linewidths with respect to wavelength, and can be designed to emit over restricted [5, 14] or wide polar angles [10, 15]. Thermal emission can also be enhanced by coupling to magnetic polaritons to obtain narrowband emission over wide polar angles [16].

In certain applications, for instance as an emitter in TPV systems or as a selective solar absorber, it is however more advantageous to broaden the bandwidth of emittance ε such that high ε is obtained at wavelengths λ below a certain cutoff wavelength λ_c while maintaining low ε at $\lambda > \lambda_c$ over all polar angles and polarizations. In this respect, metamaterial designs based on metal–dielectric stacks [17] and 2D metallic pyramid arrays [18] show great promise. However, they are difficult to fabricate and have not been experimentally demonstrated at high temperatures under extended operation. In this investigation, we present a simpler approach based on dielectric-filled anti-reflection coated (ARC) 2D metallic photonic crystals (MPhCs) to obtain omnidirectional, polarization insensitive, wavelength selective thermal emission.

2. Design and optimization

The traditional unfilled 2D MPhCs consists of a 2D square array of cylindrical holes with radius r, depth d, and period a etched into a polished flat metal. Cavity resonances of the holes are exploited to achieve selective emission [9, 11], whereby λ_c is determined by the fundamental cavity resonance frequency. This relatively simple design allows one to simultaneously achieve high ε at wavelengths $\lambda < \lambda_c$ as well as ε almost as low as a polished metal at $\lambda > \lambda_c$, with a sharp cutoff separating the two regimes. ε of the 2D MPhCs can easily be optimized for a particular application via Q-matching [19], whereby the absorptive and radiative rates of the PhC's cavity resonances are matched. In addition, any highly reflective metallic material, for instance platinum, silver, tantalum, etc. can be used since the magnitude of the first ε peak is controlled solely by Q-matching. Of the various refractory metals available, tantalum (Ta) is an excellent choice given its ultra low ε at $\lambda > \lambda_c$ and high temperature stability; hence Ta is our material of choice. To date, 2D TaPhCs have been demonstrated to be thermally stable at high temperatures in high vacuum environments [20]. In addition, the fabrication process is scalable to large areas [21].

In this investigation, rigorous coupled wave analysis methods (RCWA) [22] were used to obtain the reflectance, which allowed us to infer ε via Kirchoff's law. The Lorentz–Drude model of Ta fitted to experimentally measured ε at room temperature was used in the simulations. To ensure accuracy, the number of Fourier expansion orders were doubled until the results converged. We have also confirmed that simulations using conventional finite-difference time-domain (FDTD) methods [23] agree very well with RCWA formulations based on both polarization decomposition and normalized vector basis when more than 320 Fourier expansion orders were used.

#212642 - $15.00 USD Received 23 May 2014; revised 12 Aug 2014; accepted 12 Aug 2014; published 29 Aug 2014

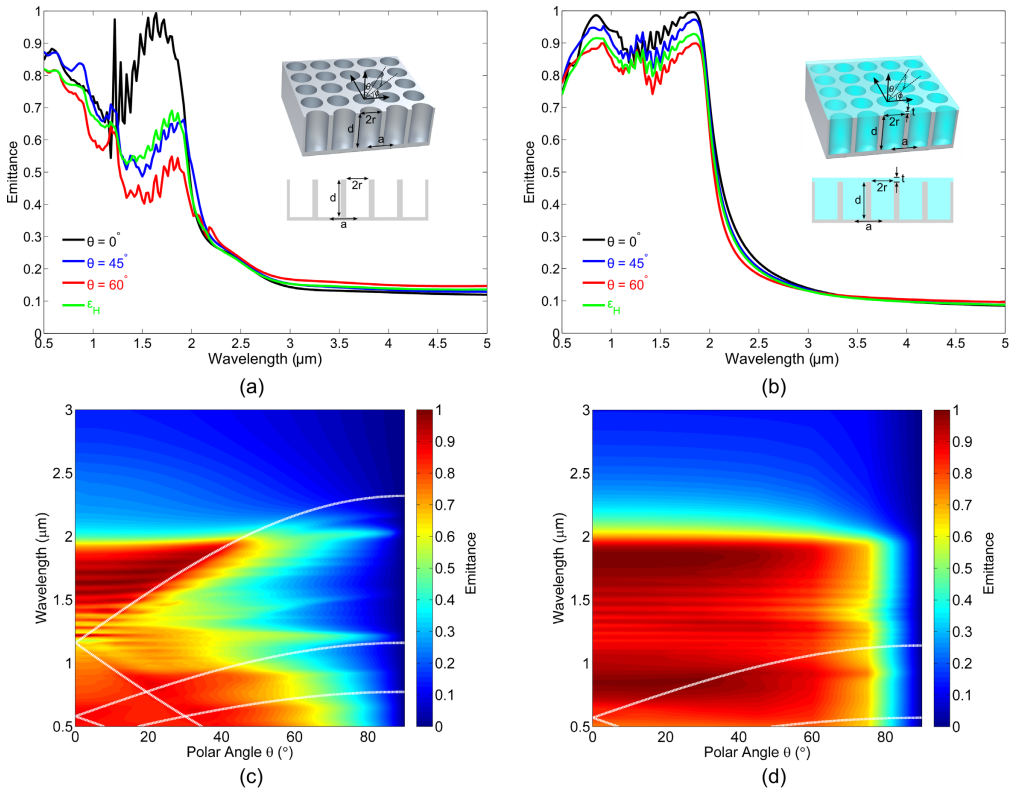

Fig. 1. Emittance ε as a function of wavelength λ and polar angle θ averaged over azimuthal angle ϕ and over all polarizations for optimized (a) 2D TaPhC (r = 0.53 μm, d = 8.50 μm, a = 1.16 μm) and (b) HfO_2-filled ARC 2D TaPhC (r = 0.23 μm, d = 4.31 μm, a = 0.57 μm, t = 78 nm). Both are optimized for λ_c = 2.00 μm. HfO_2 is depicted by the cyan-coloured areas in the inset, and ε_H is the hemispherically averaged emittance. Contour plots of $\varepsilon(\lambda,\theta)$ are also shown for optimized (c) 2D TaPhC and (d) HfO_2-filled ARC 2D TaPhC. White lines indicate the diffraction thresholds as defined by Eq. (2).

While Q-matching can successfully be used to maximize the magnitude of the first ε peak, it is merely a local optimum as it is impossible to satisfy Q-matching for all higher order modes simultaneously. In other words, ensuring maximum ε for the first resonance peak does not translate into maximum broadband ε at wavelengths $\lambda < \lambda_c$, which is our goal in this investigation. In fact, the optimization problem is highly non-convex marked by a large number of local optima. Therefore, we rely on non-linear global optimization methods as local search algorithms may potentially get trapped in a localized peak [24]. In this investigation, the global optimum was found via the multi-level single-linkage method, which executes a quasi-random low-discrepancy sequence of local searches [25] using constrained optimization by linear approximation [26]. Other global search algorithms, such as the controlled random search algorithm [27], also yield similar results. The global optimization routines were implemented via NLOpt, a free software packaged that allows comparison between various global optimization algorithms [28]. In all optimization routines, the design provided by Q-matching of the fundamental mode was used as the initial estimate. In addition, the following constraints were implemented: $a - 2r \geq 100$ nm to ensure integrity of sidewalls; $d \leq 8.50$ μm based on fabrica-

#212642 - $15.00 USD Received 23 May 2014; revised 12 Aug 2014; accepted 12 Aug 2014; published 29 Aug 2014

tion limits [21].

Figures 1(a) & 1(c) show ε as a function of λ and polar angle θ averaged over azimuthal angle ϕ and over all polarizations for the unfilled 2D TaPhC optimized for maximum ε at $\lambda < \lambda_c = 2.00\,\mu m$ and minimum ε at $\lambda > \lambda_c$. As can be seen, average ε at $\lambda < \lambda_c$ for the unfilled 2D TaPhC falls dramatically as θ increases, thus severely reducing its selectivity. To understand this phenomenon, let us first review the fundamentals of a diffraction grating, which is governed by the following grating equation:

$$a(\sin\theta_i + \sin\theta_m) = m\lambda, \;\; m = \pm 1, \pm 2, \pm 3, ... \tag{1}$$

where θ_i is the radiation's angle of incidence and θ_m is the angle where the m-th order diffraction lies. The onset of diffraction occurs when m = 1 and θ_m = 90°. Thus, at normal incidence ($\theta_i = 0°$), diffraction order(s) is (are) present for $\lambda \leq a$. For radiation with a specific λ incident on the PhC, diffraction sets in when θ_i is larger than the cutoff angle given below:

$$\theta_d = \sin^{-1}\left(\frac{\lambda}{a} - 1\right) \tag{2}$$

As an example, radiation with λ = 2 μm will get diffracted when $\theta_i > \theta_d = 46.4°$ for the design shown in Fig. 1(a). Above the diffraction threshold, ε decreases because there are more channels to couple into, resulting in a smaller radiative Q, thus destroying Q-matching. This effect is clearly observed in Fig. 1(c) as indicated by the white lines, which are the diffraction thresholds as determined by Eq. (2). Therefore, at larger incident θ's, the hemispherically averaged emittance ε_H at $\lambda < \lambda_c$ decreases.

We have reported in [29] that ε_H of the 2D TaPhCs can easily be enhanced by filling the cylindrical cavities with an appropriate dielectric, thereby increasing θ_d by virtue of a reduced r, d, and hence a to obtain the same λ_c. Here, we consider an additional coating of the same dielectric with thickness t that enhances ε at $\lambda < \lambda_c$ by functioning as an anti-reflection coating (ARC). In addition, we further optimize the design using non-linear global optimization methods to uncover the best possible performance for this architecture, i.e. maximum ε at $\lambda < \lambda_c$ and minimum ε at $\lambda > \lambda_c$. With these improvements, a relative increase of up to 15% is seen for ε at $\lambda < \lambda_c$ compared to the results reported in [29].

Hafnium oxide (HfO_2) is the dielectric material of choice in this investigation because of its transparency in the visible and infrared (IR) region, compatible thermal expansion coefficient, and stability at high temperatures. HfO_2 can also be easily deposited via atomic layer deposition (ALD) [20], and sol-gel deposition methods [30]. In addition, the HfO_2 layer promotes stable operation at high temperatures by preventing detrimental chemical reactions that attack the metallic surface, and preventing geometry deformation due to surface diffusion [20, 30]. In all simulations, the refractive index n of HfO_2 have been assumed to be 1.9 for $0.50\,\mu m < \lambda < 5.00\,\mu m$, which is consistent with results reported in literature [31], as well as with our measurements of HfO_2 thin films deposited via ALD [20].

Results of the optimization for λ_c = 2.00 μm are shown in Figs. 1(b) & 1(d). As can be seen, the optimized HfO_2-filled ARC 2D TaPhC more closely approaches the ideal cutoff emitter ($\varepsilon = 1$ at $\lambda < \lambda_c$ and $\varepsilon = 0$ at $\lambda > \lambda_c$); ε is essentially unchanged up to $\theta = 40°$ and is $\gtrsim 0.8$ for $\theta < 70°$, a significant improvement compared to the unfilled 2D TaPhC. In addition, ε at $\lambda > \lambda_c$ is lower by ≈ 0.03 primarily due to smaller surface fraction of dielectric to metal. The HfO_2-filled ARC coated 2D TaPhC can also be easily optimized for different λ_c's as illustrated in Fig. 2. There is also the added flexibility of using other suitable dieletric materials, for instance silicon dioxide (SiO_2) which has $n \approx 1.45$ [32]. As shown in Fig. 3, optimized HfO_2-filled and SiO_2-filled ARC 2D TaPhCs show very similar performance. However, when using dielectrics with smaller n's, larger r, d, a, and t are necessary to achieve optimal performance as shown in Table 1.

#212642 - $15.00 USD Received 23 May 2014; revised 12 Aug 2014; accepted 12 Aug 2014; published 29 Aug 2014

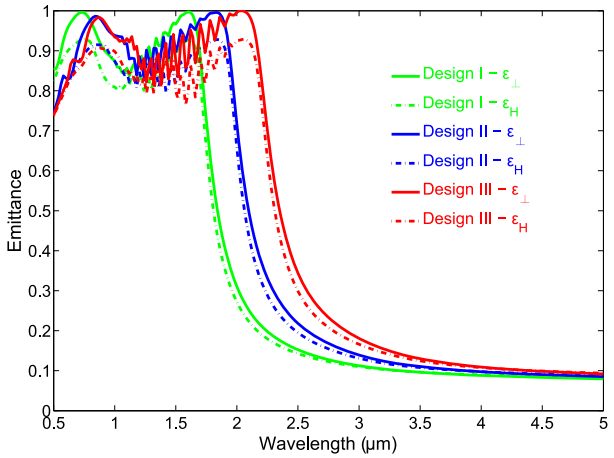

Fig. 2. Optimized HfO_2-filled ARC coated 2D TaPhC designs for λ_c = 1.70 μm (Design I: r = 0.19 μm, d = 3.62 μm, a = 0.49 μm, t = 63 nm), λ_c = 2.00 μm (Design II: r = 0.23 μm, d = 4.31 μm, a = 0.57 μm, t = 78 nm), and λ_c = 2.30 μm (Design III: r = 0.27 μm, d = 5.28 μm, a = 0.64 μm, t = 80 nm). $\varepsilon_\perp$ is $\varepsilon(\lambda, \theta = 0^\circ)$.

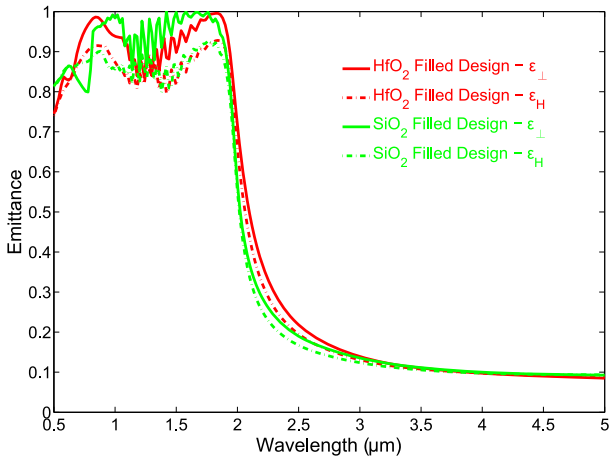

Fig. 3. Comparison between optimized HfO_2-filled ($n \approx 1.9$) and SiO_2-filled ($n \approx 1.45$) ARC 2D TaPhCs for λ_c = 2.00 μm. Similar performance is obtained, albeit at a penalty of larger r, d, a, and t when using dielectrics with smaller n as shown in Table 1.

Table 1. Relevant dimensions of the dielectric-filled ARC 2D TaPhCs optimized for λ_c = 2.00 μm using different dielectric material choices.

Dielectric	r (μm)	d (μm)	a (μm)	t (nm)
Air (n = 1)	0.53	8.50	1.16	N/A
SiO_2 (n = 1.45)	0.35	6.28	0.80	125
HfO_2 (n = 1.90)	0.23	4.31	0.57	78

#212642 - $15.00 USD Received 23 May 2014; revised 12 Aug 2014; accepted 12 Aug 2014; published 29 Aug 2014

3. Application: thermophotovoltaic energy conversion

In this section, we illustrate the optimization of the HfO_2-filled ARC 2D TaPhC for an example application: selective emitters in an InGaAsSb TPV energy conversion system. The numerical model outlined in [1] is used to obtain the following figure of merit:

$$\text{FOM} = x\eta_{\text{TPV}} + (1-x)\frac{J_{\text{elec}}^{\text{PhC}}}{J_{\text{elec}}^{\text{BB}}} \tag{3}$$

where $J_{\text{elec}}^{\text{PhC}}/J_{\text{elec}}^{\text{BB}}$ captures the TPV system power density performance of the PhC selective emitter compared to the blackbody, and x is the weighting given to the radiant heat-to-electricity efficiency η_{TPV} in the optimization routine. Here, we are mainly concerned in obtaining the highest possible η_{TPV}, thus $x = 0.9$ is used. Results of the optimization for temperature T = 1250 K with view factor of 0.99 achievable with 100 mm $\times$ 100 mm flat plate geometry with emitter-TPV cell separation of 500 μm for various selective emitter and cold-side filter combinations are shown in Table 2. Note that when used at high T, a much smaller d of 750 nm is sufficient for optimum performance due to increased intrinsic ε of Ta, of which lends itself to easier fabrication. Our ongoing investigations include actual fabrication of this structure for TPV applications.

Table 2. Comparison of η_{TPV} and J_{elec} between a greybody emitter (ε = 0.9), optimized unfilled 2D TaPhC (r = 0.57 μm, d = 4.00 μm, a = 1.23 μm), and optimized HfO_2-filled ARC 2D TaPhC (r = 0.22 μm, d = 0.75 μm, a = 0.73 μm, t = 146 nm) in InGaAsSb thermophotovoltaic (TPV) systems at T = 1250 K and view factor $F = 0.99$ (achievable with 100 mm $\times$ 100 mm flat plate geometry with emitter-TPV cell separation of 500 μm) with or without a cold-side filter.

Emitter	Filter	η_{TPV} (%)	J_{elec} (W/cm^2)
Greybody (ε = 0.9)	N/A	6.38	0.781
Optimized 2D TaPhC	N/A	12.03	0.621
Optimized HfO_2-filled ARC 2D TaPhC	N/A	12.71	0.713
Greybody (ε = 0.9)	10 layer Si/SiO_2	12.52	0.700
Optimized 2D TaPhC	10 layer Si/SiO_2	18.31	0.568
Optimized HfO_2-filled ARC 2D TaPhC	10 layer Si/SiO_2	19.34	0.646
Greybody (ε = 0.9)	Rugate Tandem Filter	23.44	0.726
Optimized 2D TaPhC	Rugate Tandem Filter	23.68	0.588
Optimized HfO_2-filled ARC 2D TaPhC	Rugate Tandem Filter	23.76	0.671

In TPV systems without a cold side filter, the optimized HfO_2-filled ARC 2D TaPhC enables up to 99% and 6% relative improvement in η_{TPV} over the greybody emitter ($\varepsilon = 0.9$) and the optimized unfilled 2D TaPhC respectively. More importantly, up to 15% relative improvement is seen in J_{elec} with the optimized HfO_2-filled ARC 2D TaPhC compared to the unfilled 2D TaPhC due to 26% relative improvement in ε_{H} at $\lambda < \lambda_{\text{c}}$. The improved electrical power density is especially vital in many portable power applications where power generated per kilogram of weight (W/kg) is the primary figure of merit. This improvement in J_{elec} is observed even when the 10 layer Si/SiO_2 filter [33] or Rugate tandem filter [34] is included on the front side of the TPV cell. Note that as state-of-the-art Rugate tandem filters are used, the improvement in η_{TPV} from implementing MPhCs over a greybody becomes insignificant. Nevertheless, Rugate tandem filters are extremely expensive; specialty materials (antimony selenide, antimony sulfide, gallium telluride, highly doped indium arsenide phosphide) are used, and a large number of

#212642 - $15.00 USD Received 23 May 2014; revised 12 Aug 2014; accepted 12 Aug 2014; published 29 Aug 2014

layers are required ($\simeq$ 100 layers). In contrast, the optimized HfO_2-filled ARC 2D TaPhC & 10 layer Si/SiO_2 cold-side filter combination may be a cheaper alternative to realizing cheaper, more scalable, yet efficient TPV energy conversion systems.

4. Conclusion

In summary, we have demonstrated optimized designs of dielectric-filled ARC 2D MPhCs for omnidirectional, polarization insensitive, broadband wavelength selective emission. The optimized designs possess high ε_{H} of 0.86 at $\lambda < \lambda_{\text{C}}$ and low ε_{H} of 0.12 at $\lambda > \lambda_{\text{C}}$, whereby λ_{C} can easily be shifted and optimized via non-linear global optimization tools. These designs provide the platform necessary for many applications, including solar absorbers for solar thermal applications, selective emitters in TPV energy conversion systems, and near- to mid-IR radiation sources for IR spectroscopy.

Acknowledgments

This work is partially supported by the Army Research Office through the Institute for Soldier Nanotechnologies under Contract No. W911NF-13-D-0001. Y. X. Y., J. B. C., S.-G. Kim, and M. S. are partially supported by the MIT S3TEC Energy Research Frontier Center of the Department of Energy under Grant No. DE-SC0001299. V. R. gratefully acknowledges funding by the Austrian Science Fund (FWF): J3161-N20. The authors would also like to thank Jay Senkevich for valuable discussions.

#212642 - $15.00 USD Received 23 May 2014; revised 12 Aug 2014; accepted 12 Aug 2014; published 29 Aug 2014